Journal of
Analytical & Bioanalytical Techniques

Yan et al., J Anal Bioanal Tech 2015, 6:6
DOI: 10.4172/2155-9872.1000290

Research Article Open Access

# A Novel Catechol Electrochemical Sensor Based on Cobalt Hexacyanoferrate/(CoHCF)/Au/SBA-15

**Yaqian Yan, Linjing Wu, Qianqiong Guo and Shasheng Huang***
*Life and Environmental Science College, Hanghai Normal University, Shanghai, PR China*

**Abstract**

A novel electrochemical sensor for catechol was developed by electrodepositing $HAuCl_4$ and cobalt hexacyanoferrate (CoHCF) on an ordered mesoporous SBA-15 decorated glassy carbon electrode (GCE). The CoHCF/Au/SBA-15 film was characterized by scanning electron microscopy (SEM) and impedance spectra. A mesoporous SBA-15 was used as a platform that enlarged the surface area of the working electrode. The CoHCF/Au/SBA-15 modified electrode showed good electrocatalytic activity to catechol and the electrocatalytic response was measured using cyclic voltammetry and Amperometric *i-t* curve. The electrochemical performance of the sensor for catechol was further enhanced due to the deposition of Au on the electrode surface. Under the optimal conditions, the sensor showed a linear range from $3.0 \times 10^{-7}$M to $5.1 \times 10^{-5}$M of catechol, with a detection limit of 50 nM (S/N=3). Good reproducibility, stability and good selectivity in the presence of numerous organic phenolics made the CoHCF/Au/SBA-15 modified electrodes applicable to the determination of catechol in the various water samples.

**Keywords:** Cobalt hexacyanoferrate; Mesoporous molecularsieve; Catechol; Amperometric i-t curve

## Introduction

Recent decades, considerable efforts have been invested in the determination of phenolic compounds in environmental, industrial, agricultural, and food fields [1,2]. Phenolic compounds are released into environment by a large number of industries, such as coal mining, oil refinery, paint, polymer and pharmaceutical preparation. Phenolic compounds are secondary metabolites. They are not involved in growth and energy metabolism and are usually generated in response to environmental stress [2]. Some of these phenolic compounds like phenol, hydroquinone, are also harmful to humans and animals [3]. Catechol (CC, 1,2-dihydroxybenzene) is a phenolic derivative with several applications such as an antifungal preservative on potato plantations, a photographic and fur dye developer, and as an antioxidant [4]. Therefore, the determination of catechol is very important in environmental protection. Catechol undergoes oxidation under mild conditions to give benzoquinone. Benzoquinone is said to be antimicrobial, which slows the spoilage of wounded fruits and other plant parts. Catechol is produced by the reversible two-electron, two-proton reduction of 1,2-benzoquinone (Scheme 1) [5].

Catechol contains phenolic hydroxy group and possesses excellent electrochemical activity. Many electrochemical methods using different modified electrodes have been reported for the determination of catechol [6-8].

Transition metal hexacyanoferrates (MHCFs) belong to a class of polynuclear inorganic mixed-valence compounds because of their reversible redox properties and their zeolitic structure [9-12], the color of prussian blue (PB) or iron (III) hexacyanoferrate (II) can be reversibly switched by electrochemical treatments [13]. Among the many transition metal hexacyanoferrates, cobalt hexacyanoferrate (CoHCF) has interesting chemical and electrochemical properties [14-17], which makes it a suitable modifier in many sensing applications. CoHCF exhibits well-defined and reproducible electrochemical responses at not only oxidized but also reduced states [10]. In addition, CoHCF film can also be easily fabricated on various electrode substrates [13] and CoHCF modified electrode shows good electrocatalytic activity toward a variety of substrates [14-17].

Gold nanoparticles (AuNPs) exhibit distinctive physical, chemical and catalytic properties because of their size, shape and high surface to volume ratio in contrast to bulk materials [18]. In particular, Gold nanoparticles have received much attention because of their applications in catalysis, nanoelectronics, drug delivery and chemical sensing [19]. Recently, increasing attention is being given to the fabrication of thin films of metal nanoparticles from both a fundamental and a practical application point of view. Such thin films of metal nanoparticles on solid surfaces have been prepared using a number of strategies including assembly techniques with cross linkers for metal nanoparticles [20].

Mesoporous materials are the focus of research due to their porous structure and high surface area, and the past decade many innovative synthetic methods of the mesoporous materials have been developed employing self-assembled surfactants as structure-directing agents [21-23]. Porous silicon (PS) has emerged as a promising material for sensor applications since it presents a number of advantages like miniaturization, integration of signal processing circuitry, low cost, greater surface area, and greater adsorption capacity [24-26]. They showed remarkable applications such as in molecular sieves, adsorbents, gas sensors, protein immobilization, etc. [27-31].

In this paper, the mesoporous SBA-15 was synthesized and the electrochemical behaviors of the glassy carbon electrode modified with CoHCF-Au nanocomposites based on mesoporous SBA-15 were investigated. The experimental results of the present work indicated that the CoHCF/Au/SBA-15 modified electrode showed an improved electrochemistry response to catechol compared with that without SBA-

***Corresponding author:** Shasheng Huang, Life and Environmental Science College, Hanghai Normal University, Shanghai, 200234, PR China, Tel: +86-021-64321828; Fax: +86-021-64321828; E-mail: sshuang@shnu.edu.cn

**Received** October 12, 2015; **Accepted** October 29, 2015; **Published** November 05, 2015

**Citation:** Yan Y, Wu L, Guo Q, Huang S (2015) A Novel Catechol Electrochemical Sensor Based on Cobalt Hexacyanoferrate/(CoHCF)/Au/SBA-15. J Anal Bioanal Tech 6: 290. doi:10.4172/2155-9872.1000290

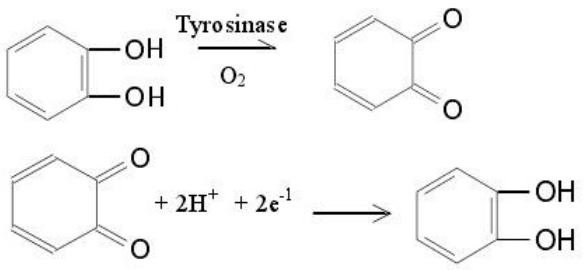


**Scheme 1:** Reaction for Catechol production.

15 due to the greater surface area of SBA-15 as the substrate material. Electrochemical results showed that the CoHCF-Au nanocomposites in the gaps of SBA-15 could enhance the direct electron transfer. The catechol sensor was successfully used in real waste water sample analysis with a stability and reliable recovery.

## Experimental

### Apparatus and reagents

All chemicals and reagents used in the study were of A.R. grade and used as received without further purification. Catechol ($C_6H_6O_2$, 99%), tetraethoxysilane (TEOS, 98%), hydrochloric acid (HCl, 37%) and pluronic copolymer P123 (non-ionic triblock copolymer, $EO_{20}PO_{70}EO_{20}$, MW=5800) were purchased from Sigma Chemicals Company. Gold (III) chloride trihydrate ($HAuCl_4{\cdot}3H_2O$, 99.9%), cobalt chloride hexahydrate ($CoCl_2{\cdot}6H_2O$, 99.9%) were obtained from Aldrich. Phosphate buffer solution (PBS, 0.1M) was used to prepare the supporting electrolyte and the pH value was adjusted by mixing the stock solution of $NaH_2PO_4$ and $Na_2HPO_4$. Prior to experiments, the solutions were purged with purified nitrogen for at least 15 min to remove oxygen. Milli Q 18.2 MΩ water was used throughout the experiments.

The cyclic voltammetric measurements were carried out on CHI760B electrochemical workstation (Chen Hua Instrument, Shanghai, China). A conventional three electrode system was used in this work consists of CoHCF/Au/SBA-15/GCE as the working electrode, a thin Pt wire as auxiliary electrode and saturated calomel electrode (SCE) as the reference electrode. All the experiments were conducted at room temperature unless otherwise stated. Scanning electron microscopy (SEM) measurements were carried out using a JSM 6360 LV microscope (JEOL Ltd, Japan) operating at 100 kV. The transmission electron micrograph (TEM) was obtained using a JEM-2100 TEM instrument (JEOL). Fourier transformation infrared (FT-IR) spectra (4000-400 $cm^{-1}$) in KBr were obtained with a Vector 22 FTIR spectrometer (Bruker Optics, Germany). X-ray diffraction (XRD) patterns were collected on a Bruker D8 Advance X-ray diffractometer (Bruker, Germany).

### The synthesis of mesoporous SBA-15

The synthesis of SBA-15 was conducted as described in the literature [22,23]. In a typical preparation, 4.0 g P123 was completely dissolved in 130 g ultrapure water, and 20 mL HCl solution (37%) was added with stirring at 35°C. Then 8.5 g TEOS was slowly added to the solution with stirring at 35°C for 24 h. The mixture was then transferred to an autoclave and aged for 24 h at 80°C. The solid product was recovered by filtration, washed with ultrapure water, and air-dried at room temperature. Calcination was carried out in an air atmosphere at 550°C for 6 h with a heating rate of 1°C/min to remove the template and the final product was denoted as mesoporous SBA-15.

### Fabrication of CoHCF/Au/SBA-15/GCE

The GCE was carefully polished with 1.0, 0.3 and 0.05 μm alumina powder successively, followed by rinsing thoroughly with ultrapure water. The polished electrode was sonicated in acetone and water, respectively. Then the cleaned GCE was pretreated by scanning from - 0.2 to 1.2 V in 0.5 M $H_2SO_4$ and dried at room temperature. The as-prepared SBA-15 (4.0 mg) was dispersed into 2 ml DMF and the mixture was sonicated for 1 h to form a stable white suspension.

The fabrication of CoHCF/Au/SBA-15/GCE was performed as follows: Firstly, 4.0 μL SBA-15 solution was dropped onto the pretreated glassy carbon electrode surface and dried in air. Secondly, Au nanoparticles were immobilized on electrode surface by cyclic voltammetry in 0.1% $HAuCl_4$ between 0 and 1.6 V at scan rate of 50 $mV{\cdot}s^{-1}$, then the electrode was washed with water and dried in air (this electrode was denoted as Au/SBA-15/GCE). The Au/SBA-15/GCE was scanned from -0.2 to 1.3 V at 50 $mV{\cdot}s^{-1}$ in 1.0 mM $CoCl_2$ solution (containing 0.05M KCl), potassium ferrocyanide solution (1.0 mM), with 0.1 M KCl as the background electrolyte to get a thin film of CoHCF on the surface. Unless otherwise stated, the procedure involved 10 full voltammetric cycles (20 segments) in the potential range from -0.2 to 1.3 V. After cycling, the electrode was kept at the potential of 1.3 V for 20 min to get deposition of cobalt hexacyanoferrate (CoHCF) [32]. After being removed from the solution and thoroughly rinsed with water, the electrode was dried in air for later use. The obtained electrode was the CoHCF/Au/SBA-15 /GCE. The preparation process of this sensor is shown in Scheme 2.

### Sample preparation and measurement procedures

All experiments were carried out at room temperature and high purity nitrogen was kept flowing over the solution during the experiments. Solutions of catechol (99%, Sigma-Aldrich) were prepared daily. Under the optimal conditions, CV was conducted in 10.0 mL PBS (0.1M, pH=6.98) and CV was carried out between -0.3 to 0.5 V at scan rate of 100 $mV{\cdot}s^{-1}$. The determination of catechol in the samples was performed using *i-t* curve with initial potential of 0.4 V.

## Results and Discussion

### Characterization of SBA-15

The crystalline structure and the phase composition of SBA-15 were characterized by X-ray diffraction (XRD). The small-angle XRD pattern for as-synthesized SBA-15 prepared with $EO_{20}PO_{70}EO_{20}$ showed three well-resolved diffraction peaks in the 2θ range 0.5-5°,

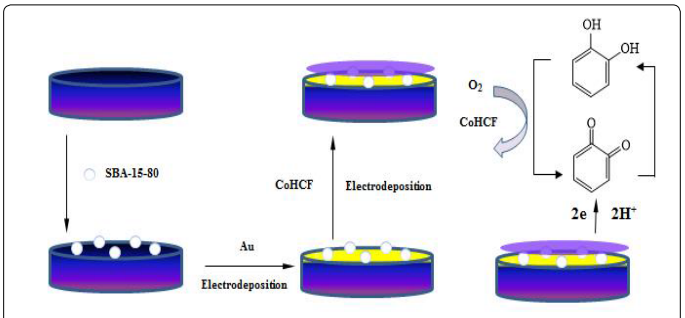


**Scheme 2:** Preparation of the catechol sensor and the proposed mechanism of the sensor for catechol electrocatalytic detection.

which corresponded to the diffraction of (100), (110), and (200) planes, respectively [33] (Figure 1), indicating that as-synthesized SBA-15 had a high degree of hexagonal mesoscopic organization. These diffraction peaks were characteristic of the ordered structure of SBA-15.

Scanning electron microscopy (SEM) images (Figure 2A) revealed that the as-synthesized SBA-15 sample was consists of many rope-like domains with relatively uniform sizes, which were typical microstructures of the mesoporous SBA-15. Transmission electron microscopy (TEM) images (Figure 2B) of calcined SBA-15 showed well-ordered hexagonal arrays of Mesopores and further confirmed that SBA-15 had a 2D p6mm hexagonal structure.

The $N_2$-sorption studies of SBA-15-X samples exhibited type IV isotherms according to IUPAC classification with H1 hysteresis loop, which were characteristics of mesoporous materials with one-dimensional cylindrical channels [34]. A pore diameter of 6.24 nm (Figure S1 in the supporting information), and a Brunauer-Emmett-Teller (BET) surface area of 518 $m^2 \cdot g^{-1}$ can be observed. Three well distinguished regions of the adsorption isotherm (Figure S1 in the supporting information) were apparent: (i) monolayer multilayer adsorption, (ii) capillary condensation and (iii) multilayer adsorption on the outer particle surfaces.

## Characterization of the modified electrode

The modified CoHCF/Au composite was characterized by scanning electron microscopy (SEM). Figure 3A showed that bare GCE was clean and smooth and the mesoporous SBA-15 had typically rod structures (Figure 2A). After Au nanoparticles and cobalt hexacyanoferrate (CoHCF) were electrodeposited on the Bare GCE, as seen in Figure 3B, the CoHCF/Au composite presented a clear nano-flower structure on the electrode. And these assembled materials were evenly dispersed on glassy carbon electrode.

EIS (Electrochemical impedance spectroscopy) was employed to reveal the impedance changes of the corresponding electrode surface. The frequency varied from 105 to 0.05 Hz and the ac excitation amplitude was 5 mV. Figure 4 shows the Nyquist plots for the electrodes in a 0.1 M KCl solution containing 1 mM $[Fe(CN)_6]^{4-/3-}$(1:1).

From the Figure 4, it can be seen that the Ret for bare GCE was 600 Ω (curve a GCE). After modification of SBA-15, the value of Ret significantly increased to 4230 Ω (curve b SBA-15/GCE), as a result of the existence of the mesoporous silica skeleton which has poor conductivity. After electropolymerization of Au nanoparticles on SBA-15 surface, the value of Ret immediately increased to 156.4 Ω, indicating that the introduction of AuNPs could improve electron transfer kinetics to a large extent in the self-assembly process of the sensor (curve c Au/SBA-15/GCE). After the introduction of transition metal ferricyanide (CoHCF), the value of Ret of the sensor was larger than that of Au/ SBA-15/GCE maybe the conductivity of CoHCF was weaker than AuNPs (curve d CoHCF/Au/SBA-15/GCE).

Figure 5 showed the cyclic voltammograms obtained for differently modified electrodes in 1mM $[Fe(CN)_6]^{3-/4-}$ aqueous solution containing 0.1M KCl at scan rate of 100 $mV \cdot s^{-1}$. The CVs showed well-defined typical diffusion-limited patterns, The bare glassy carbon electrode (GCE) witnessed a pair of well-defined redox peaks with the anodic ($E_{pa}$) and cathodic ($E_{pc}$) peak potential of 0.159 V and 0.233 V, respectively, and a peak potential difference of 74 mV (Figure 5, curve a). These peaks could be definitely attributed to the redox behaviors of $[Fe(CN)_6]^{3-/4-}$. The modification of SBA-15 on electrode surface induced a big decrease of peak current, which was invoked by the

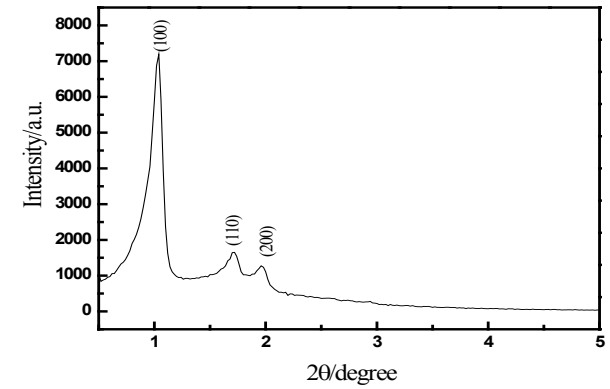


**Figure 1:** Low-angle powder X-ray diffraction patterns of SBA-15 materials.

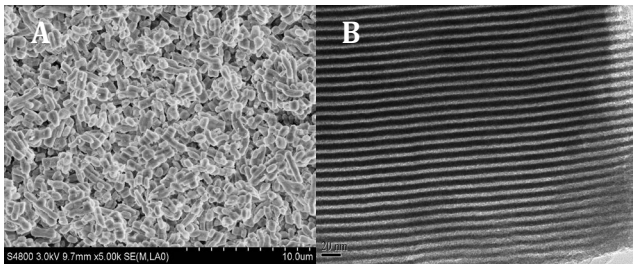


**Figure 2:** SEM image (A) and TEM image of SBA-15(B).

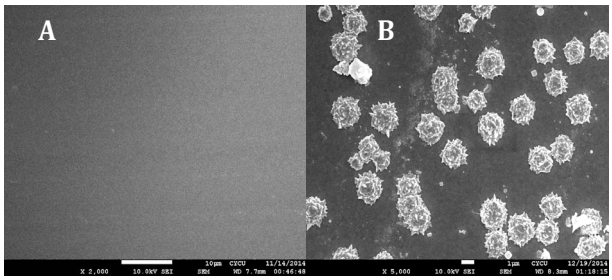


**Figure 3:** SEM image of bare GCE (A) and CoHCF/Au/ GCE (B).

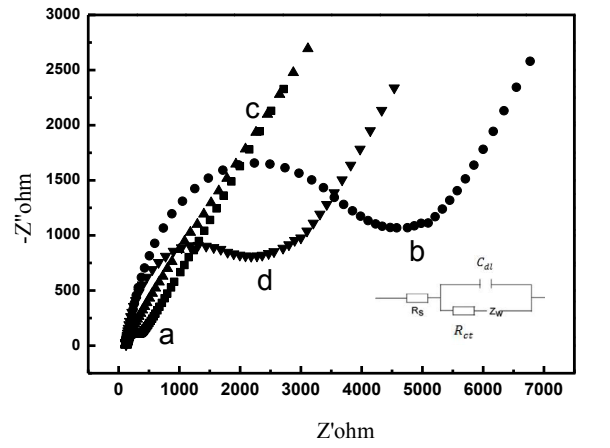


**Figure 4:** Electrochemical impedance spectra of bare GCE (a), SBA-15/GCE(b), Au/ SBA-15/GCE (c) and CoHCF/Au/SBA-15/GCE (d).

diffusion inhibition of $[Fe(CN)_6]^{3-/4-}$ to the electrode surface (Figure 5, curve b). The Au nanoparticles modification was convinced to increase the effective electrode surface area and the rate of electron transfer at the sensor, which was confirmed by an apparent increase in the voltammetric responses of $[Fe(CN)_6]^{3-/4-}$ than that of SBA-15 modified electrode (Figure 5, curve c). Nevertheless, the further assembly of CoHCF on the Au/SBA-15 modified electrode obviously decreased the peak current of $[Fe(CN)_6]^{3-/4-}$ as observed in curve d, which could be reasonable considering that the electron transfer $[Fe(CN)_6]^{3-/4-}$ to the underlying electrode surface was partially blocked. At the other extreme, indicating that CoHCF has been successfully immobilized onto the GCE modified with SBA-15. The results of the cyclic voltammetric experiments for differently modified electrodes were in good agreement with the results by impedance experiments.

Figure 6 shows the current responses obtained for the different decorated electrodes in o.1 mM catechol solution in a potential range of -0.3-0.5 V. The CVs showed the bare GCE (a) and SBA-15/GCE (b) had small redox current responses to catechol. While the current responses of Au/SBA-15/GEC (c), CoHCF/Au/SBA-15/GCE (d) and CoHCF/Au/GCE (e) were all larger than that of Curve a, b, which indicated that the deposition of Au on the electrode surface could increase the electron transfer rate, enhance electrical conductivity and made the current signal large. As seen in Curve c and d, CoHCF showed good electrocatalytic activity toward catechol. Besides, CVs of CoHCF/Au/SBA-15/GCE (d) and CoHCF/Au/ GCE (e) depicted that the decorated electrode showed larger current response to the catechol.

## Electrodeposition processes of Au nanoparticles and cobalt hexacyanoferrate (CoHCF)

The electropolymerization of Au nanoparticles on SBA-15 surface was done by continuous potential cycling for 10 cycles in the range of 0.0 V to 1.6 V. The continuous growth of Au nanoparticles exhibited two redox processs [36]. The results showed CVs obtained at SBA-15/GCE in 0.2% $HAuCl_4$ at scan rate of 120 $mV{\cdot}s^{-1}$ (Figure S2 in the supporting information). Two quasi-reversible redox waves were observed at SBA-15/GCE in the potential range of 0.0 V and 1.6 V. Both the redox peak currents and the peak-to-peak difference increase with increasing scan rates. It can be seen that the consequential increase of the redox peak currents when the potential scan rate is increased. In order to achieve appropriate AuNPs, scan rate of 50 $mVs^{-1}$ was chosen for the immobilization of Au nanocomposites.

CoHCF was electrodeposited from the solutions containing 1.0 mM $CoCl_2$ solution, 1 mM $K_3[Fe(CN)_6]$ and 0.1M KCl. Before the electrodeposition, CVs were recorded in $K_3[Fe(CN)_6]$ at different scan rates to estimate the effective electrode area. The cyclic voltammograms showed that the deposition of CoHCF nanoparticles started at a potential where the reduction of $[Fe(CN)_6]^{3-}$ to $Fe(CN)_6^{4-}$ occurred, and then $Co^{2+}$ reacted instantaneously with $[Fe(CN)_6]^{4-}$ to form CoHCF nanoparticles on the electrode surface (Figure S3 in the supporting information). Before the electrodeposition, the reversible peaks of the $[Fe(CN)_6]^{3-}/[Fe(CN)_6]^{4-}$ system were recorded. Three well-defined reversible peaks were detected around 0.60 V. CoHCF was discovered to grow with each potential cycle, as revealed by the increasing of peak currents with each cycle. An apparent voltammetric change was observed in the deposition process of CoHCF. The redox peak currents of the electrode increase with increasing the segment number.

## Optimization of experimental conditions

**Effect of scan rate:** The influence of potential scan rate on the electrochemical behavior of catechol at GCE was studied [37] (Figure 6A). The relationship between current (i) versus scan rate at the modified electrode was studied individually in the presence of 0.1 mM catechol. When the sensor was cycled between 20 and 180 $mV{\cdot}s^{-1}$, a linear relationship was obtained between the peak intensity $I_{pa}$ and the scan rate $v$ (Figure 6B), indicating that the oxidation of catechol at GCE is a adsorption controlled process. In addition, the anodic peak potential shifted to positive values with the scan rate increased and these results also confirmed that the oxidation reaction was irreversible.

**Effect of pH:** The effect of pH on the response of catechol at the sensor was investigated by recording the cyclic voltammograms in the range of -0.4-0.6 V at a scan rate of 100 $mV{\cdot}s^{-1}$. The anodic peak currents for catechol increased with the increase of pH from 4.5 to 7.0 (Figure 7A) and reached a maximum value at 7.0. When the pH value is higher than 7.0, the peak current decreases rapidly. Within these pH ranges, the relationship between pH and the anodic peak potential was investigated (Figure 7B). It can be seen that the peak potential is shifted to less positive values as the pH of the solution increasing from 4.5 to 8.0 for catechol. These results indicated that protons are participating

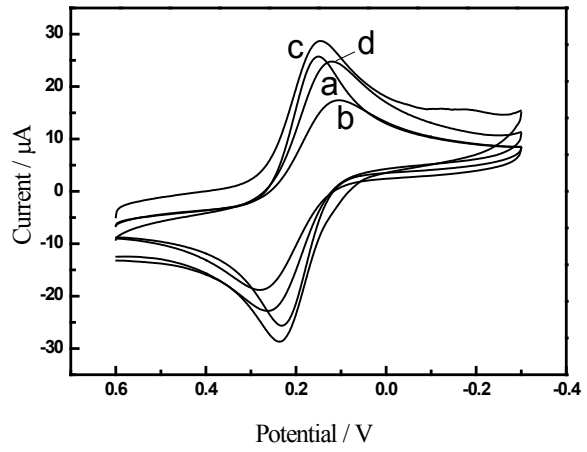


**Figure 5:** Cyclic voltammograms of the bare electrode (a), SBA-15/GEC (b), Au/SBA-15/GEC (c) and CoHCF/Au/SBA-15/GCE (d).

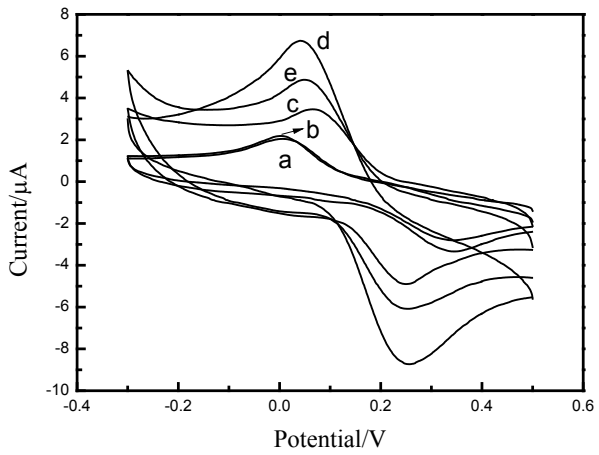


**Figure 6:** CV curves of the bare electrode (a), SBA-15/GEC (b), Au/SBA-15/GEC (c), CoHCF/Au/SBA-15/GCE (d) and CoHCF/Au/ GCE (e) in 0.1mM catechol (pH=7.0).

in the oxidation of catechol. The plot of $E_{pa}$ vs. pH showed a straight line. The equation for peak potential with pH for catechol is expressed as follows:

$E_{pa}$=0.6433-0.058 pH (R=0.999)

The slope of ≈59 mV·pH$^{-1}$ unit is indicative of single electron transfer processes involving one proton according to the Nernst relationship.

## Chronocoulometry studies of the GCE and modified electrodes

The electrochemical effective surface area for the bare GCE and CoHCF/Au/SBA-15/GCE can be calculated by the slope of the plot of $Q$ vs. $t^{1/2}$ obtained by chronocoulometry using $[Fe(CN)_6]^{3-}$ as a model complex (the diffusion coefficient $D$ of $[Fe(CN)_6]^{3-}$ is $7.6 \times 10^{-6}$ cm$^2$·s$^{-1}$ [38]) The corresponding $Q$–$t$ curves and $Q$-$t^{1/2}$ plots were also performed and shown in Figure 8. This was according to the formula given by Anson [38] (1):

$$Q(t) = \frac{2nFAcD^{1/2}t^{1/2}}{\pi^{1/2}} + Q_{dl} + Q_{ads} \quad (1)$$

where $A$ is the surface area of the working electrode, $c$ is the concentration of substrate, $D$ is the diffusion coefficient, $Q_{dl}$ is double layer charge which could be eliminated by background subtraction, and $Q_{ads}$ is Faradic charge. Based on the slope of the linear relationship between $Q$ and $t^{1/2}$, $A$ can be calculated to be 0.00116 cm$^2$ and 0.00297 cm$^2$ for the GCE and CoHCF/Au/SBA-15/GCE, respectively (Figure 8B). The results indicated that the electrode effective surface area was increased obviously after modification of the GCE with CoHCF/Au/SBA-15/GCE, which could enhance the total adsorption capacity of catechol, leading to the increase of current response of catechol, decreasing the limit of detection (Figure 9).

## Amperometric determination of CC at CoHCF/Au/SBA-15/GCE

Figure 9 illustrates the real-time amperometric $i$-$t$ curve of CoHCF/Au/ SBA-15/GCE with successive addition of catechol to a continuously stirred PBS (pH=7.0) solution under optimized experimental conditions. Oxidation current was increased with increasing the catechol concentration. The maximum steady-state current of the sensor was achieved within 4 s. The result indicating that it is a fast

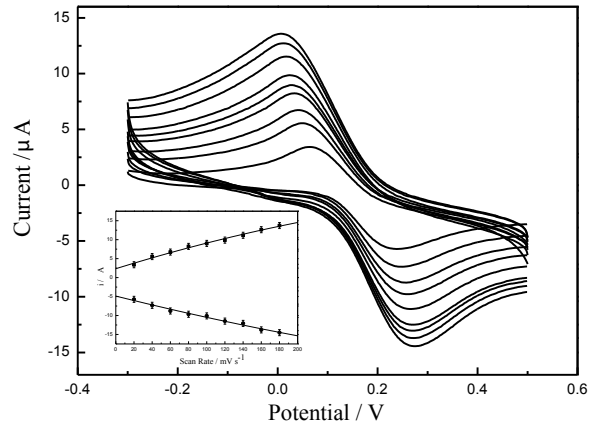


**Figure 7:** (A) CV curves of 0.1mM catechol in 0.1M PBS (pH=7.0), containing 0.1M KCl at different scan rates: 20, 40, 60, 80, 100, 120, 140, 160, 180 mVs$^{-1}$. (B) Dependence of peak current on the scan rate.

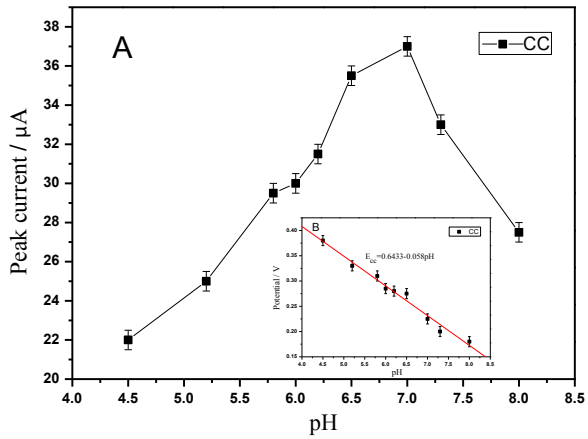


**Figure 8:** Effect of pH on anodic peak current for 0.1mM catechol. Insert: dependence of anodic peak potential on pH.

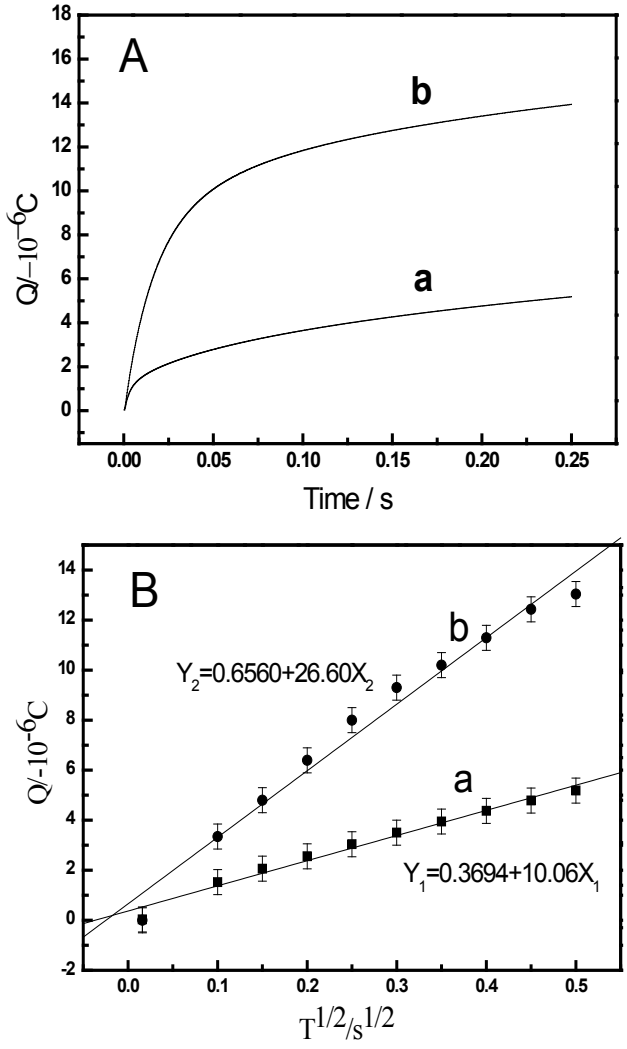


**Figure 9:** (A) Plot of $Q$–$t$ curves for the GCE (a) and CoHCF/Au/SBA-15/GCE (b) in 0.1mM $K_3Fe(CN)_6$ solution containing 0.1mM KCl. (B)Linear relationship of $Q$–$t^{1/2}$ on the GCE (a) and CoHCF/Au/SBA-15/GCE (b).

oxygen reduction reaction. The regression equation of linear current response with catechol concentration is $i(\mu A)=0.44619c+0.00213$ (μM) (R=0.999). The CoHCF/Au/SBA-15/GCE displays a linear response range from $3.0 \times 10^{-7}$ to $5.1 \times 10^{-5}$M of catechol with the detection limit of 5 nM (S/N=3). Conspicuously, the detection limits, sensitivity, and applied potential obtained in the present work exhibited comprehensive superior than other sensors were summarized in Table 1.

## Reproducibility durability and selectivity of the modified electrode

Reproducibility of the catechol sensor was investigated with the measurement of the modified electrode in $4.83 \times 10^{-6}$M target catechol solution. Three catechol sensors, made independently, showed the response current values of $5.05 \times 10^{-6}$A, $4.98 \times 10^{-6}$A and $5.17 \times 10^{-6}$A with a relative standard deviation of 1.89% (n=3). A RSD 5.19% (n=6) can be obtained in the continuous determination of six times. The catechol in waste water was detemined based on the amperometric *i-t* curve (Table 2). It indicated that a satisfactory reproducibility could be obtained by this system. The stability of the modified electrode was also tested. No significant changes in cathodic and anodic peaks current were observed for more than 10 complete CV cycles. When a modified electrode was stored in the 0.1M PBS buffer solution (pH=7.0) for at least one week at 4°C, the electrode retained about 95.2% of its initial response.

## Interference of coexisting substances and the practical sample analysis

The influences of common interfering species on the determination of catechol were investigated in the presence of 3.0 μM catechol with great details. Some common phenolic complexes and inorganic ions were tested to check their levels of interference in the determination of catechol (Figure 10). Interference was taken as the level causing an error in excess of 5%. It was found that most ions and common substances with high concentration, $Na^+$, $K^+$, $Fe^{3+}$, $Zn^{2+}$, $Cu^{2+}$, $NO_3^-$, $Cl^-$, $SO_4^{2-}$ and $PO_4^{3-}$, $Ca^{2+}$, $Zn^{2+}$, $Mg^{2+}$, $Pb^{2+}$ did not interfere on the determination of catechol. 150 fold Lysine, cysteine, glucose citric acid, dopamine, ascorbic acid, uric acid, 100 fold p-aminophenol, phenol, 1-nitroso-2-naphthol and 10 fold ortho-aminophenol produced a negligible change on the response currents of the sensor, indicating that the CoHCF/Au/SBA-15/GCE exhibits good selectivity for catechol detection (Figure 11).

## Conclusion

In summary, a novel electrochemical sensor with an excellent current response for the catechol based on CoHCF/Au/SBA-15 film was prepared. The sensor showed a linear relationship of $3.0 \times 10^{-7}$ to $5.10 \times 10^{-5}$M of catechol. Au nanoparticles and cobalt hexacyanoferrate (CoHCF) on the glassy carbon electrode (GCE) obviously improved the response characteristics of the catechol sensor. Results showed that the composite film has promising electrocatalytic activity toward the oxidation of catechol. High sensitivity, good selectivity, low detection limit, good repeatability and anti-interference ability, which have been verified by determination of catechol in waste water, made the proposed sensor show the promising practical application in environmental pollution test.

### Acknowledgements

This work was supported by the Project of the National Science Foundation of People's Republic of China (21275100), Shanghai Leading Academic Discipline Project (S30406) and Key Laboratory of Resource Chemistry of Ministry of Education.

| Electrode | Methods | Linear range | Detection limit(mol $L^{-1}$) | Reference |
|---|---|---|---|---|
| $SiO_2/C/Nb_2O_5$ | DPV | $3.98 \times 10^{-5}$-$9.8 \times 10^{-4}$ | $0.8 \times 10^{-6}$ | [37] |
| Au/L-lysine/OMC-Au/Tyr/GCE | DPV | $4.0 \times 10^{-7}$-$8.0 \times 10^{-5}$ | $2.5 \times 10^{-8}$ | [32] |
| Tyr/CoPc/CGCE | *i-t* | $3.0 \times 10^{-6}$-$8.63 \times 10^{-4}$ | $4.5 \times 10^{-7}$ | [38] |
| CoHCF/Au/SBA-15/GCE | *i-t* | $3.0 \times 10^{-7}$-$5.10 \times 10^{-5}$ | $5 \times 10^{-8}$ | This work |

**Table 1:** Comparison of the determination of catechol by different sensing methods.

| Sample No | Detection (μmol/L) | Addition (μmol/L) | Found (μmol/L) | Recovery (%) |
|---|---|---|---|---|
| 1 | 1.0 | 1.0 | 1.93 | 96.5 |
| 2 | 2.0 | 1.5 | 3.38 | 96.6 |
| 3 | 1.5 | 1.5 | 2.89 | 96.3 |
| 4 | 5.0 | 4.5 | 9.84 | 103.6 |
| 5 | 1.7 | 2.0 | 3.82 | 103.2 |
| 6 | 9.0 | 5.0 | 13.87 | 99.1 |

**Table 2:** Analysis of catechol in waste water samples (n=6).

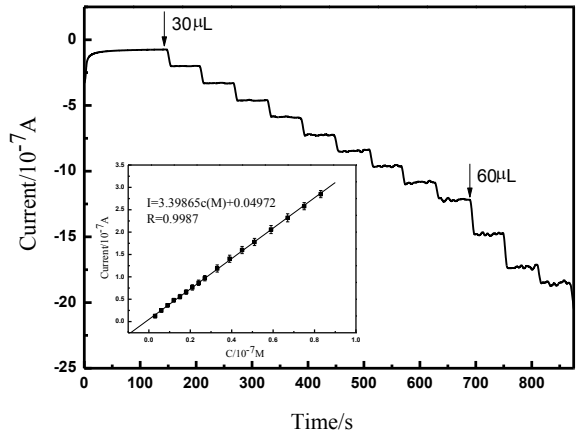


**Figure 10:** Amperometric response obtained on the CoHCF/Au/SBA-15/GCE upon successive addition of catechol at different concentrations to 0.1M PBS (pH=7.0) with applied potential at 0.15 V. Inset: calibration curves of the catechol sensor.

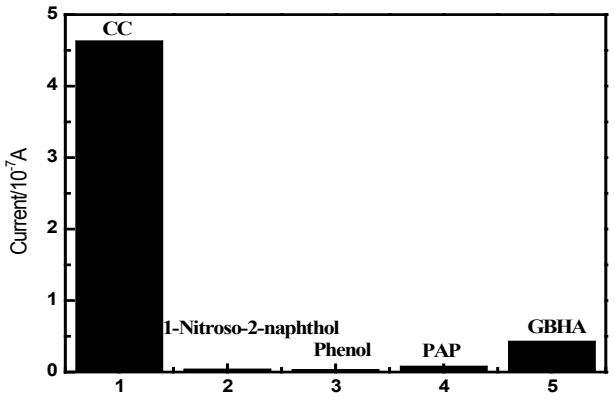


**Figure 11:** Current response histogram of 3.0 μM catechol and organic phenolics at CoHCF/Au/SBA-15/GCE.

## References

1. Yang K, Chen XH, Ni JH, Yao SP, Wang WC, et al. (2010) Palygorskite-expanded graphite electrodes for catalytic electro-oxidation of phenol. Applied Clay Science 49: 64-68.
2. Harnly JM, Bhagwat S, Lin LZ (2007) Profiling methods for the determination of phenolic compounds in foods and dietary supplements. Anal Bioanal Chem 389: 47-61.
3. Irons RD (1985) Quinones as toxic metabolites of benzene. J Toxicol Environ Health 16: 673-678.
4. Bukowska B, Kowalska S (2004) Phenol and catechol induce prehemolytic and hemolytic changes in human erythrocytes. Toxicol Lett 152: 73-84.
5. Du HJ, Ye JS, Zhang JQ, Huang XD, Yu CZ (2011) A voltammetric sensor based on graphene-modified electrode for simultaneous determination of catechol and hydroquinone. Journal of Electroanalytical Chemistry 650: 209-213.
6. Tang L, Zhou Y, Zeng G, Li Z, Liu Y, et al. (2013) A tyrosinase biosensor based on ordered mesoporous carbon-Au/L-lysine/Au nanoparticles for simultaneous determination of hydroquinone and catechol. Analyst 138: 3552-3560.
7. Canevari TC, Arenas LT, Landers R, Custodio R, Gushikem Y (2013) Simultaneous electroanalytical determination of hydroquinone and catechol in the presence of resorcinol at an SiO2/C electrode spin-coated with a thin film of Nb2O5. Analyst 138: 315-324.
8. Carralero V, Mena ML, Gonzalez-cortés A, Pingarron JM (2006) Development of a high analytical performance-tyrosinase biosensor based on a composite graphite-Teflon electrode modified with gold nanoparticles. Biosensors and Bioelectronics 22: 730-736.
9. Liu J, Lin YH, Liang L, Voigt JA, Huber DL, et al. (2003) Templateless Assembly of Molecularly Aligned Conductive Polymer Nanowires: A New Approach for Oriented Nanostructures. Chemistry-A European Journal 9: 604-611.
10. Xun Z, Cai C, Lu T (2004) Effects of a Surfactant on the Electrocatalytic Activity of Cobalt Hexacyanoferrate Modified Glassy Carbon Electrode Towards the Oxidation of Dopamine. Electroanalysis 16: 674-683.
11. Tao WY, Pan DW, Liu YG, Nie LH, Yao SZ (2004) Characterization and electrocatalytic properties of cobalt hexacyanoferrate films immobilized on Au-colloid modified gold electrodes. Journal of Electroanalytical Chemistry 572: 109-117.
12. Haghighi B, Varma S, Alizadeh Sh FM, Yigzaw Y, Gorton L (2004) Prussian blue modified glassy carbon electrodes-study on operational stability and its application as a sucrose biosensor. Talanta 64: 3-12.
13. DeLongchamp DM, Hammond PT (2004) Multiple-Color Electrochromism from Layer-by-Layer-Assembled Polyaniline/Prussian Blue Nanocomposite Thin Films. Chemistry of Materials 16: 4799-4805.
14. Golabi SM, Noor-Mohammadi F (1998) Electrocatalytic oxidation of hydrazine at cobalt hexacyanoferrate- modified glassy carbon, Pt and Au electrodes. Journal of Solid State Electrochemistry 2: 30-37.
15. Cai CX, Xue KH, Xu SM (2000) Electrocatalytic activity of a cobalt hexacyanoferrate modified glassy carbon electrode toward ascorbic acid oxidation. Journal of Electroanalytical Chemistry 486: 111-118.
16. Chen SM (1998) Characterization and electrocatalytic properties of cobalt hexacyanoferrate films. Electrochimica Acta 43: 3359-3369.
17. Cataldi TRI, Benedetto GD, Bianchini A (1999) Enhanced stability and electrocatalytic activity of a ruthenium-modified cobalt–hexacyanoferrate film electrode. Journal of Electroanalytical Chemistry 471: 42-47.
18. Daniel MC, Astruc D (2003) Gold Nanoparticles: Assembly, Supramolecular Chemistry, Quantum-Size-Related Properties, and Applications toward Biology, Catalysis, and Nanotechnology. Chemical Reviews 104: 293-346.
19. Saha K, Agasti SS, Kim C, Li X, Rotello VM (2012) Gold nanoparticles in chemical and biological sensing. Chem Rev 112: 2739-2779.
20. Shipway AN, Willner I (2001) Nanoparticles as structural and functional units in surface-confined architectures. Chem Commun (Camb): 2035-2045.
21. Beck JS, Vartuli JC, Roth WJ, Leonowicz ME, Kresge CT, et al. (1992) A new family of mesoporous molecular sieves prepared with liquid crystal templates. Journal of the American Chemical Society 114: 10834-10843.
22. Zhao D, Feng J, Huo Q, Melosh N, Fredrickson GH, et al. (1998) Triblock copolymer syntheses of mesoporous silica with periodic 50 to 300 angstrom pores. Science 279: 548-552.
23. Zhao DY, Feng JL, Cmelka BF, Stucky GD, Huo QS (1998) Nonionic Triblock and Star Diblock Copolymer and Oligomeric Surfactant Syntheses of Highly Ordered, Hydrothermally Stable, Mesoporous Silica Structures. Journal of the American Chemical Society 120: 6024-6036.
24. Stewart MP, Buriak JM (2000) Chemical and Biological Applications of Porous Silicon Technology. Advanced Materials 12: 859-869.
25. Lillis B, Jungk C (2005) Microporous silicon and biosensor development: structural analysis, electrical characterisation and biocapacity evaluation. Biosensors and Bioelectronics 21: 282-292.
26. Francia GD, Ferrara VL, Manzo S, Chiavarini S (2005) Towards a label-free optical porous silicon DNA sensor. Biosens Bioelectron 21: 661-665.
27. Deere J (2002) Mechanistic and Structural Features of Protein Adsorption onto Mesoporous Silicates. The Journal of Physical Chemistry B 106: 7340-7347.
28. Hartmann M (2005) Ordered Mesoporous Materials for Bioadsorption and Biocatalysis. Chemistry of Materials 17: 4577-4593.
29. Carrott MMLR, Candeias AJE, Carrott PJM, Ravikovitch PI, Neimark AV, et al. (2001) Adsorption of nitrogen, neopentane, n-hexane, benzene and methanol for the evaluation of pore sizes in silica grades of MCM-41. Microporous and Mesoporous Materials 47: 323-337.
30. Sayari A (1996) Catalysis by Crystalline Mesoporous Molecular Sieves. Chemistry of Materials 8: 1840-1852.
31. Yamada T, Zhou HS, Uchida H, Tomita M, Ueno Y, et al. (2002) Surface Photovoltage NO Gas Sensor with Properties Dependent on the Structure of the Self-Ordered Mesoporous Silicate Film. Advanced Materials 14: 812-815.
32. Prabakar SJ, Narayanan SS (2006) Surface modification of amine-functionalised graphite for preparation of cobalt hexacyanoferrate (CoHCF)-modified electrode: an amperometric sensor for determination of butylated hydroxyanisole (BHA). Analytical and Bioanalytical Chemistry 386: 2107-2115.
33. Yang CM, Kalwei M, Schüth F, Chao K (2009) Gold nanoparticles in SBA-15 showing catalytic activity in CO oxidation. Applied catalysis A: General 254: 289-196.
34. Schmidt R, Hansen EW, Stoecker M, Akporiaye D, Ellestad OH (1995) Pore Size Determination of MCM-51 Mesoporous Materials by means of 1H NMR Spectroscopy, N2 adsorption, and HREM. A Preliminary Study. Journal of the American Chemical Society 117: 4049-4056.
35. Du P, Li H, Mei Z, Liu S (2009) Electrochemical DNA biosensor for the detection of DNA hybridization with the amplification of Au nanoparticles and CdS nanoparticles. Bioelectrochemistry 75: 37-43.
36. Abolhasani J, Hosseini H, Khanmiri RH (2014) Electrochemical study and differential pulse voltammetric determination of oxcarbazepine and its main metabolite at a glassy carbon electrode. Analytical Methods 6: 850-856.
37. Heusler KE, Adams RN (1969) Electrochemistry at Solid Electrodes. Erschienen in der Buchreihe "Monographs in Electroanalytical Chemistry and Electrochemistry". Marcel Dekker Inc., New York. 402 Seiten. Berichte der Bunsengesellschaft für physikalische Chemie 73: 1098-1098.
38. Anson FC (1964) Application of Potentiostatic Current Integration to the Study of the Adsorption of Cobalt(III)-(Ethylenedinitrilo(tetraacetate) on Mercury Electrodes. Analytical Chemistry 36: 932-934.